iScience

CellPress
OPEN ACCESS

Article

A prognostic and immune related risk model based on zinc homeostasis in hepatocellular carcinoma

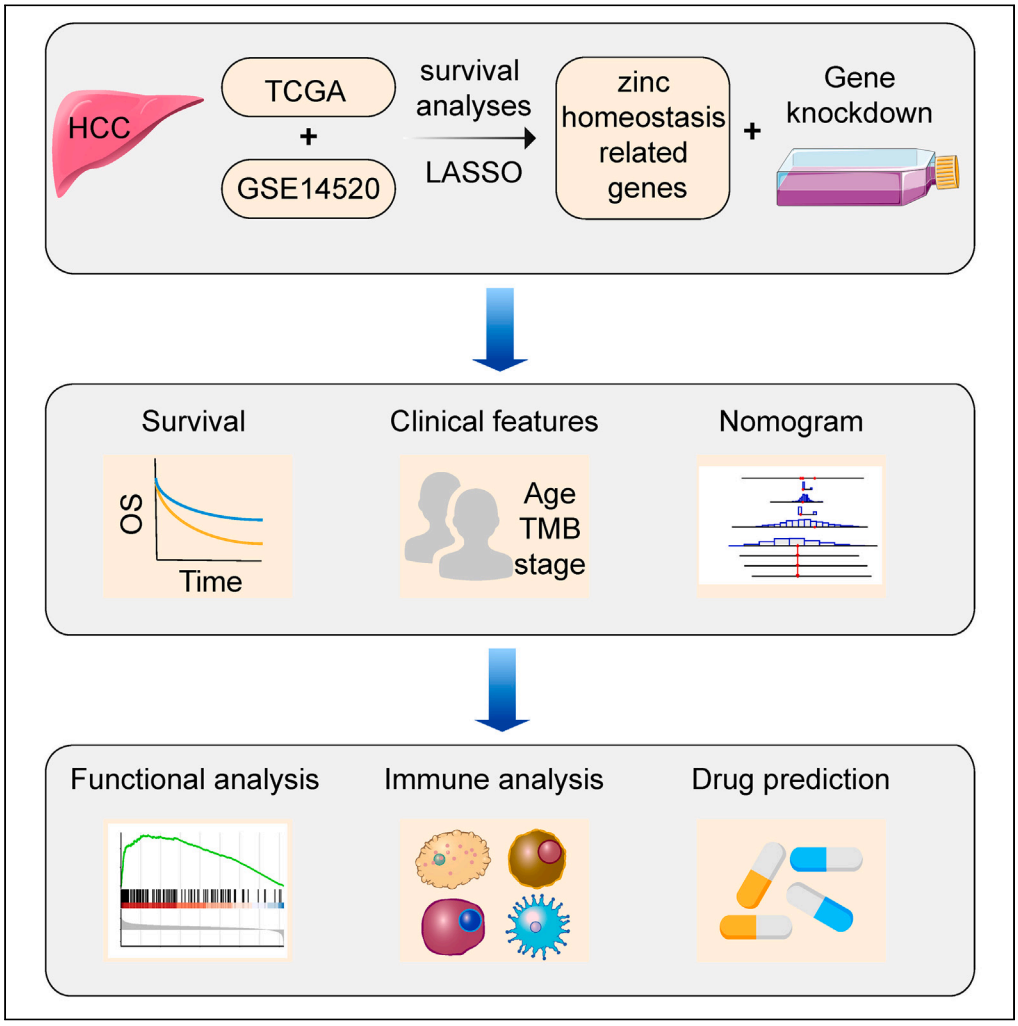

Yifei Shi, Runxin Ye, Yuan Gao, Fengyan Xia, Xiao-Fang Yu

xfyu1@zju.edu.cn

Highlights

Evaluation of the prognostic value of zinc homeostasis in HCC

UCK2 is upregulated and essential for proliferation and migration of HCC

Patients with higher risk scores are associated with immune suppression

The risk model may provide potential treatment strategies for patients with HCC

Shi et al., iScience *27*, 109389
April 19, 2024 © 2024 The Author(s).
https://doi.org/10.1016/j.isci.2024.109389

iScience

CellPress
OPEN ACCESS

Article

A prognostic and immune related risk model based on zinc homeostasis in hepatocellular carcinoma

Yifei Shi,[1,5] Runxin Ye,[1,5] Yuan Gao,[2] Fengyan Xia,[1] and Xiao-Fang Yu[1,3,4,6,*]

SUMMARY

Hepatocellular carcinoma (HCC) is the third leading cause of cancer-related deaths worldwide. The dysfunction of zinc homeostasis participates in the early and advancing malignancy of HCC. However, the prognostic ability of zinc homeostasis in HCC has not been clarified yet. Here, we showed a zinc-homeostasis related risk model in HCC. Five signature genes including *ADAMTS5*, *PLOD2*, *PTDSS2*, *KLRB1*, and *UCK2* were screened out via survival analyses and regression algorithms to construct the nomogram with clinical characteristics. Experimental researches indicated that *UCK2* participated in the progression of HCC. Patients with higher risk scores always had worse outcomes and were more associated with immune suppression according to the analyses of immune related-pathway activation, cell infiltration, and gene expression. Moreover, these patients were likely to exhibit more sensitivity to sorafenib and other antitumor drugs. This study highlights the significant prognostic role of zinc homeostasis and suggests potential treatment strategies in HCC.

INTRODUCTION

The mortality rate of liver cancer has increased in the last decade.[1] In the liver cancer, hepatocellular carcinoma (HCC) is the most prevalent type, accounting for approximately 90% of all cases.[2] The pathogenesis of HCC is critically complex with a high degree of heterogeneity, calling for the more specific molecular clarification.[3] The treatment options for HCC included surgical resection, ablation, and systemic therapies;[4] however, most patients with advanced HCC still have the poor outcomes with a 5-year survival rate of approximately 20%[1] and a recurrence rate of 70% 5 years after resection.[5] The treatment dilemma was probably due to limited long-term benefits and predictive biomarkers for immune therapies,[6] the challenge of drug resistance,[7] and the deficiency of effective drugs targeting the vital mutation of HCC.[3] Therefore, more practicable prediction models for prognosis and drug sensitivity are urgently needed.

Zinc is the necessary and abundant metallic element for the human body, regulating enzymatic activity, protein structure and stability, and gene expression.[8] The intracellular zinc homeostasis is tightly maintained by zinc transport proteins, including Zrt, Irt-related protein (ZIP) family, and Zn transporter (ZnT) family.[9,10] Zinc deficiency is associated with various pathological conditions like growth retardation, impaired wound healing, and immune dysfunction,[11] or diseases including Alzheimer's disease,[12,13] sickle cell disease,[14] and cancer.[15] The dysfunction of zinc and partial zinc transporters affects the tumorigenesis and progression of prostate cancer,[8,16] pancreatic cancer,[17] breast cancer,[18] and HCC.[19,20] Furthermore, a recent study revealed that zinc-related nanoclusters can enhance the production of reactive oxygen species and antitumor immunity against HCC in a mice model.[21] However, the prognostic role of zinc homeostasis in patients with HCC remains unknown.

In this research, we established a zinc homeostasis-related risk model in HCC based on survival and regression analyses. Five signature genes were defined and experimental researches were performed to explore the function of *UCK2* in HCC. Our risk model had predictive stability and reliability and was significantly associated with tumor microenvironment (TME) and drug sensitivity. This study has emphasized the prognostic model based on zinc homeostasis and provided potential therapy strategies for patients with HCC.

[1]Cancer Institute (Key Laboratory of Cancer Prevention and Intervention, China National Ministry of Education, Key Laboratory of Molecular Biology in Medical Sciences, Zhejiang Province, China), The Second Affiliated Hospital, Zhejiang University, School of Medicine, Hangzhou 310016, P.R. China
[2]Department of Breast and Thyroid Surgery, Shaoxing People's Hospital, Shaoxing 312035, P.R. China
[3]Zhejiang Provincial Clinical Research Center for CANCER, Hangzhou 310016, P.R. China
[4]Cancer Center of Zhejiang University, Hangzhou 310016, P.R. China
[5]These authors contributed equally
[6]Lead contact
*Correspondence: xfyu1@zju.edu.cn
https://doi.org/10.1016/j.isci.2024.109389

This is an open access article under the CC BY-NC-ND license (http://creativecommons.org/licenses/by-nc-nd/4.0/).

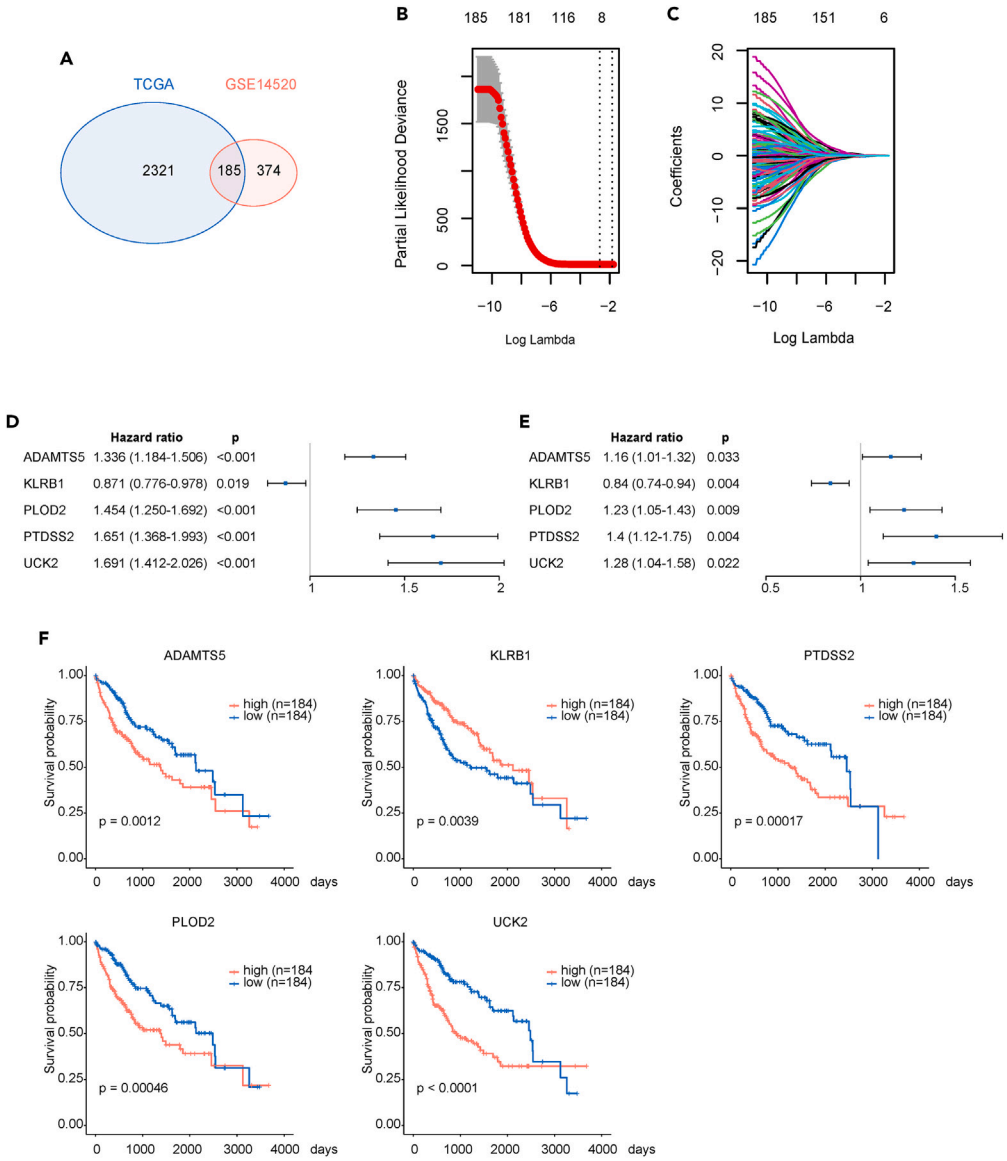

Figure 1. Identifying zinc homeostasis-related genes for constructing a prognostic risk model

(A) Intersecting genes associated with the OS of patients with HCC in the TCGA and GSE14520 cohorts.

(B and C) LASSO coefficient profiles and lambda curves of 185 intersected genes in the TCGA cohort.

(D and E) Univariate and multivariate Cox regression analysis of five signature genes to establish the optimal model.

(F) KM survival curves revealed survival difference in patients with HCC according to the expression level of five signature genes.

RESULTS

Identifying zinc homeostasis-related genes for constructing a prognostic risk model

Univariate Cox regression and Kaplan-Meier (KM) analyses were utilized to assess the relationship between the expression level of zinc homeostasis-related genes and the overall survival (OS) of patients with HCC in The Cancer Genome Atlas (TCGA) and GSE14520 cohorts. There were 2,506 genes in TCGA cohort and 559 genes in GSE14520 cohort significantly associated with OS and the number of intersecting genes was 185 (Figure 1A; Table S4). We also evaluated the expression differences of these 185 genes in the tumor and normal samples in two cohorts (Table S5). These genes were analyzed using least absolute shrinkage and selection operator (LASSO) regression and the returned 10 genes were further analyzed using multivariate Cox regression to establish an optimal prognostic model (Figures 1B and 1C). Five genes (*ADAMTS5*, *KLRB1*, *PLOD2*, *PTDSS2*, and *UCK2*) were revealed as independent prognostic elements in patients with HCC (Figures 1D and 1E). Among these genes, *ADAMTS5*, *PLOD2*, *PTDSS2*, and *UCK2* were risk factors, while *KLRB1* was a protective factor for patients

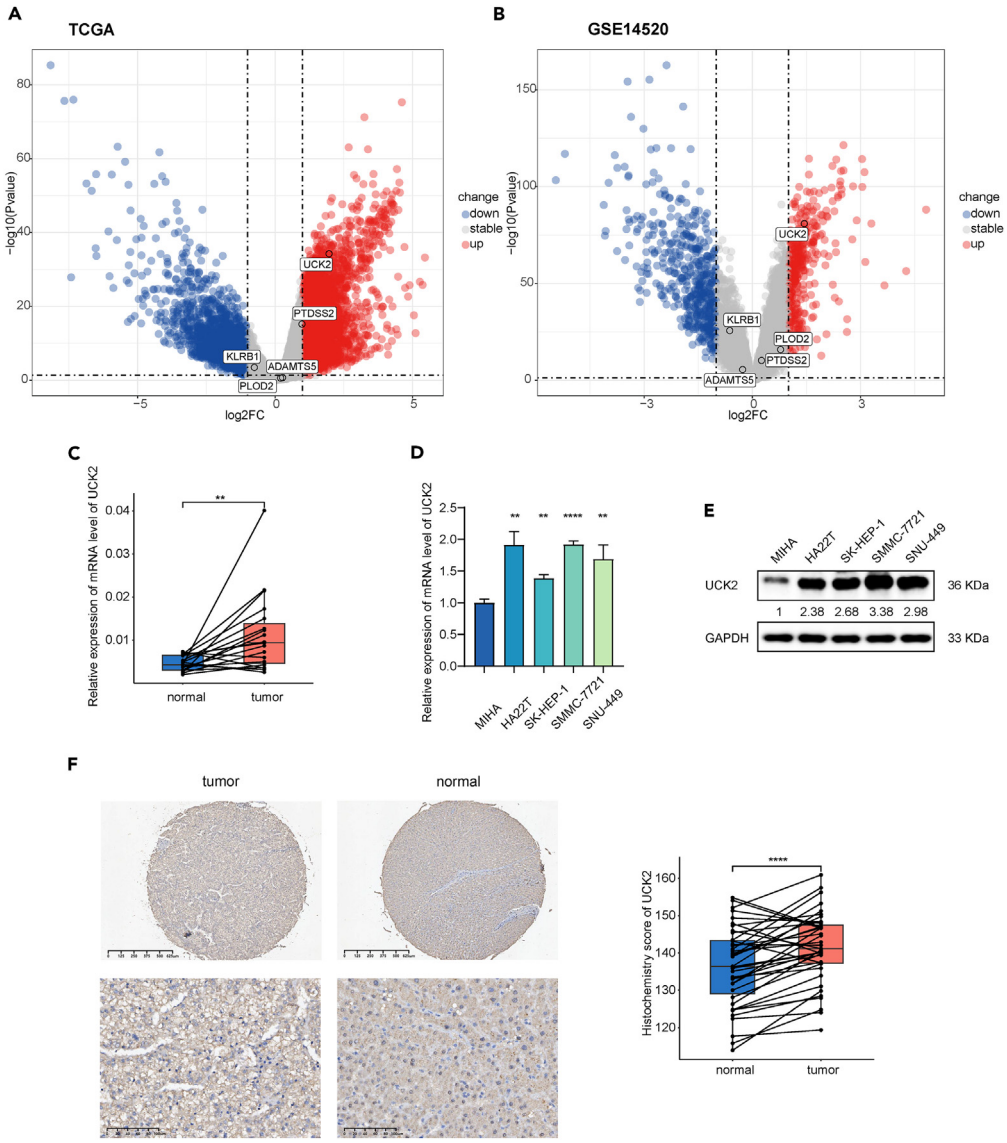

Figure 2. Validation of signature gene expression in HCC

(A and B) The volcano plots showed the expression difference of *ADAMTS5*, *KLRB1*, *PLOD2*, *PTDSS2*, and *UCK2* in tumor samples compared with normal samples in the TCGA cohort and GSE14520 cohort.

(C) The mRNA expression levels of *UCK2* in 19 paired HCC tissues and adjacent normal tissues.

(D) The mRNA expression levels of *UCK2* in normal liver cells and HCC cell lines.

(E) The protein expression levels of *UCK2* in normal liver cells and HCC cell lines.

(F) The immunohistochemistry and relative histochemistry scores of 39 matched HCC and normal tissues. (**p < 0.01, ****p < 0.0001).

with HCC (Figure 1F). The risk score was calculated as follows: risk score = (0.147 X *ADAMTS5* expression) + (−0.179 X *KLRB1* expression) + (0.204 X *PLOD2* expression) + (0.334 X *PTDSS2* expression) + (0.248 X *UCK2* expression).

Validation of signature gene expression and cellular function in HCC

The volcano plots showed that *ADAMTS5*, *KLRB1*, *PLOD2*, and *PTDSS2* were stable genes while *UCK2* was upregulated in tumor samples compared with adjacent normal samples in the TCGA and GSE14520 cohorts (Figures 2A and 2B). We then examined the expression level of *UCK2* in HCC and found that the mRNA expression of *UCK2* increased in 19 HCC samples compared with the normal samples (Figure 2C) and in HCC cell lines compared with the MIHA normal liver cell (Figure 2D). Additionally, *UCK2* also exhibited a higher protein expression level in tumor cell lines (Figure 2E) and 39 paired HCC tissues (Figure 2F). To further explore the impact of *UCK2* in HCC progression, we performed

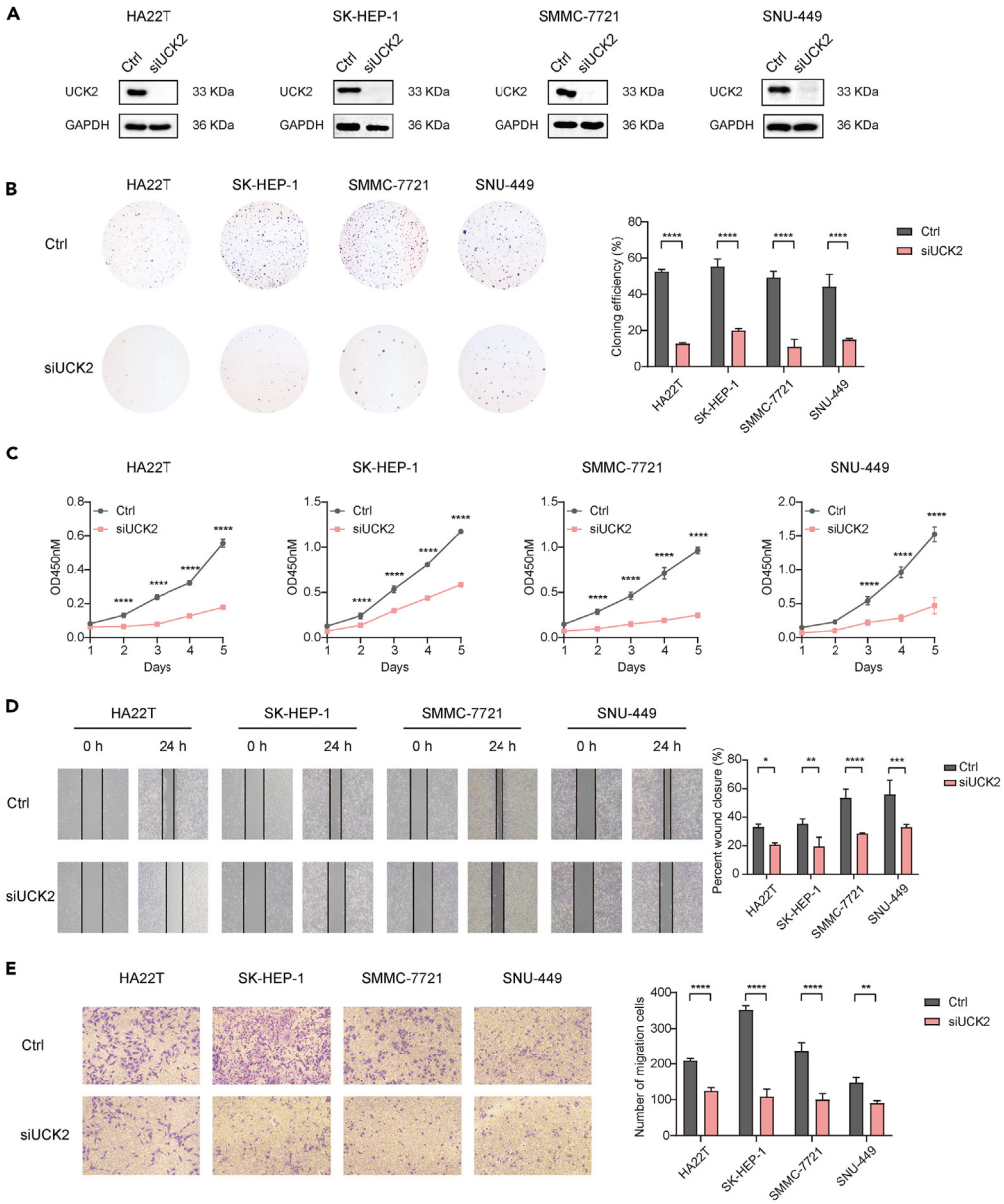

Figure 3. Validation of the impact of *UCK2* in HCC proliferation and migration

(A) Western blot showed the knockdown efficiency of *UCK2* in HCC cell lines after transfection for 48 h.

(B and C) Clone formation assay and CCK-8 assay for cell proliferation of HCC cells after transfected with *UCK2* siRNA and its scramble siRNA.

(D and E) Wound healing assay, cell migration assay, and relative quantitative results of HCC cells after knockdown of *UCK2*. (*p < 0.05, **p < 0.01, ***p < 0.001, ****p < 0.0001).

the knockdown assay in HCC cell lines and the protein expression level of *UCK2* was substantially decreased in experimental group (Figure 3A). The results of the clone formation assay and the cell counting kit-8 (CCK-8) assay showed that the knockdown of *UCK2* critically inhibited the cell proliferation in HCC (Figures 3B and 3C). Additionally, *UCK2* deficiency suppressed the migration capability of HCC cells confirmed by the wound healing assay and the migration assay (Figures 3D and 3E). These findings suggested that *UCK2* may play a vital role in HCC progression.

Prognostic potency of zinc homeostasis-related signature in the training cohort and validation cohort

In this study, we utilized the TCGA cohort as the training cohort and the GSE14520 cohort as the validation cohort to verify the predictive stability and reliability of the prognostic model. Patients were divided evenly into low-, intermediate-, and high-risk groups based on the

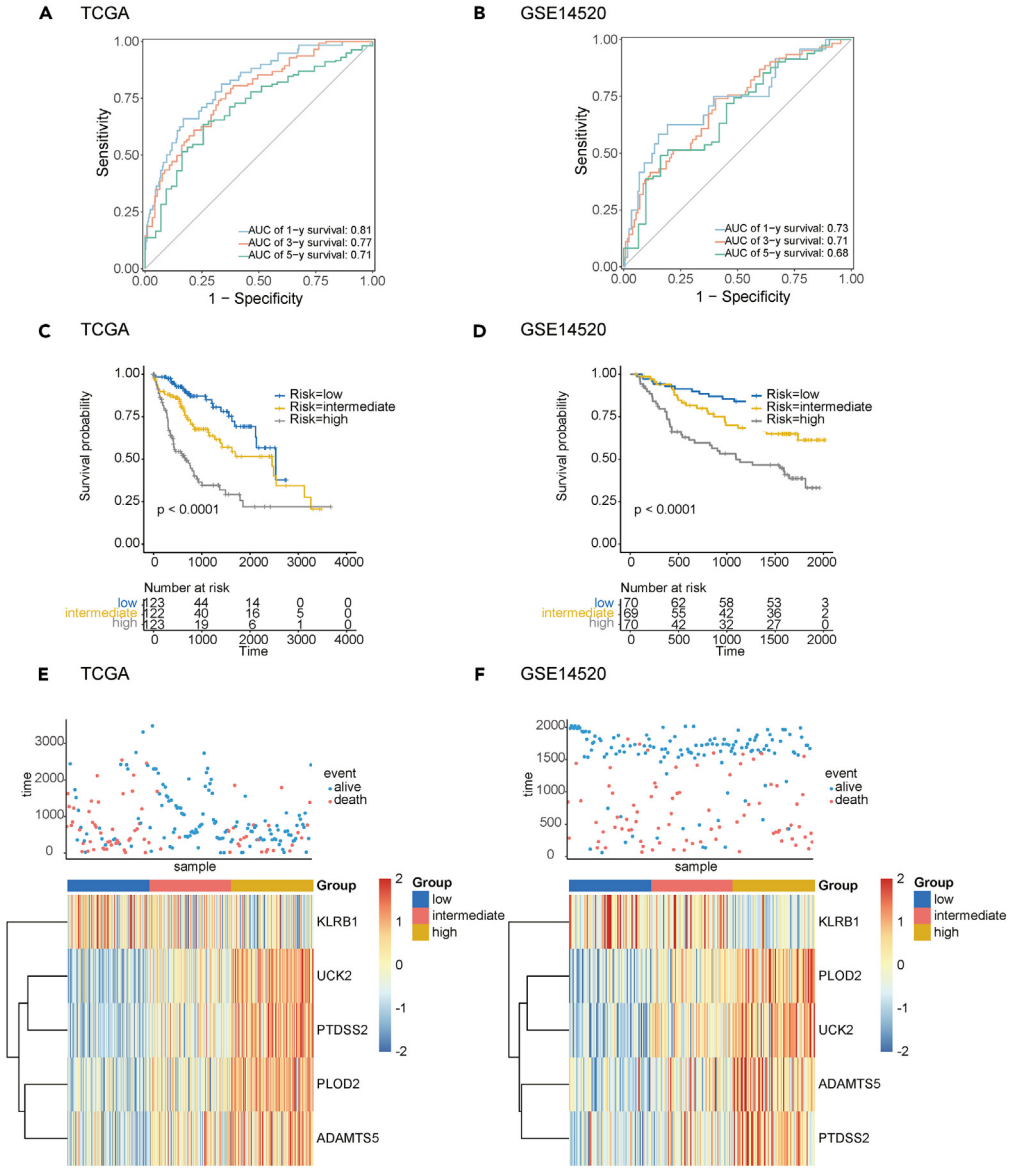

Figure 4. Prognostic potency of zinc homeostasis-related signature in the training cohort and validation cohort

(A and B) Time-dependent ROC curves of prognosis signature in the TCGA and GSE14520 cohorts.

(C and D) KM survival curves demonstrated the prognostic difference of the five gene signatures in the two cohorts.

(E and F) Distribution of the survival status of patients with HCC and related expression levels of five signature genes in the two cohorts.

risk score. Time-dependent receiver operating characteristic (ROC) curves revealed the prediction accuracy of the model. The area under the ROC curve (AUC) for 1-, 3-, and 5-year OS were 0.81, 0.77, and 0.71 in TCGA cohort and 0.73, 0.71, and 0.68 in GSE14520 cohort (Figures 4A and 4B). KM analysis indicated that patients with lower risk scores performed a better outcome (Figures 4C and 4D). Risk survival status plots revealed that the survival status and expression level of five genes for every patient in two cohorts (Figures 4E and 4F).

The nomogram based on zinc homeostasis-related signature and clinical features

As showed in Figure S1, groups were divided by stage, and age and tumor mutation burden (TMB) level remained the notable survival difference according to the risk score. The result of univariate Cox analysis demonstrated that risk score, stage, age, and TMB level were negatively related with the OS of patients (Figure 5A). Multivariate Cox analysis indicated that the risk score and grade were in connection with the OS (Figure 5B). Subsequently, the nomogram was constructed to predict the survival status (Figure 5C). The AUC for 1-, 3-, and 5-year OS were

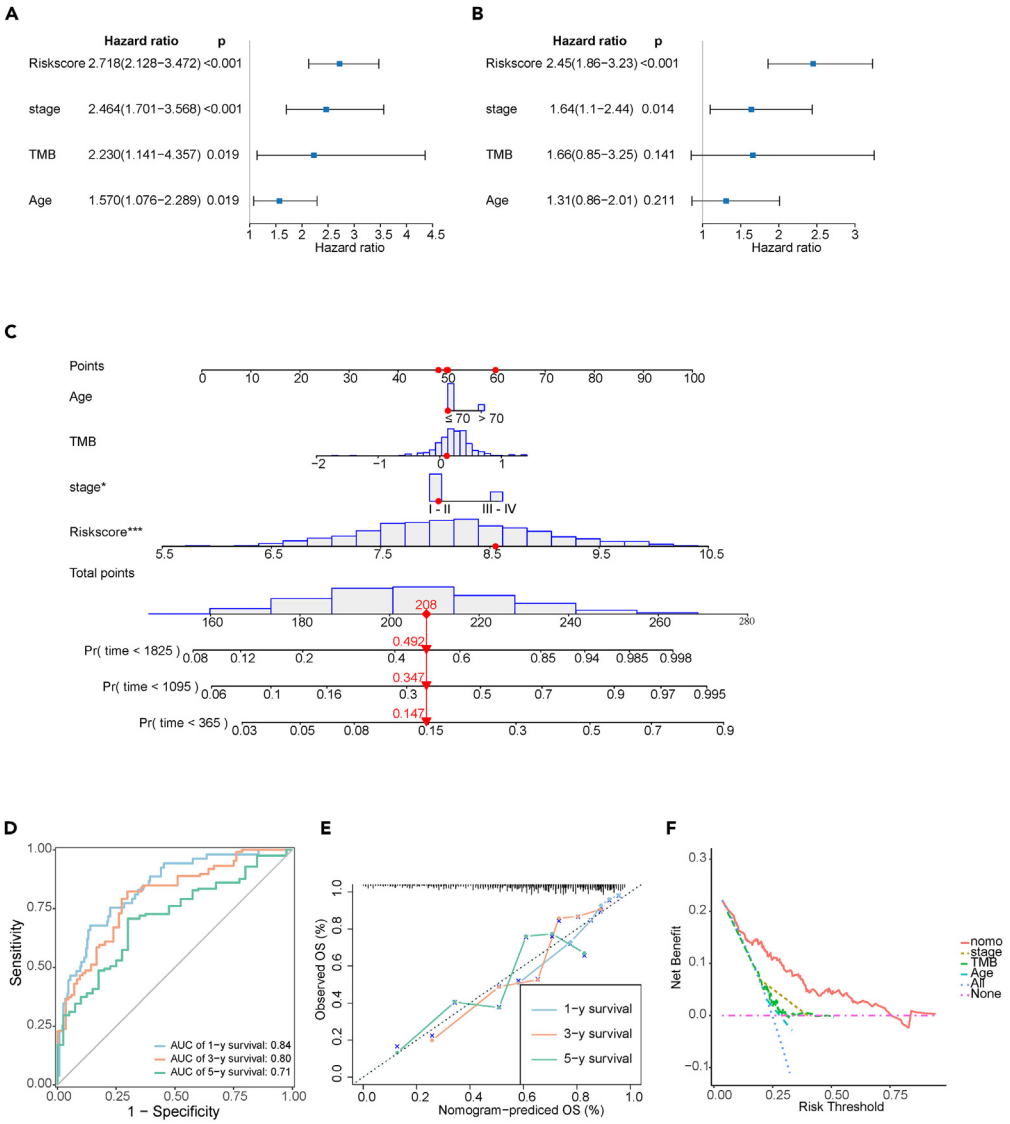

Figure 5. The nomogram based on zinc homeostasis-related signature and clinical features

(A and B) Univariate and multivariate Cox regression analysis of the risk score and other clinical characteristics including stage, age, and TMB level.

(C) Nomogram based on the risk score and clinical characteristics.

(D) Time-dependent ROC curve for 1-, 3-, and 5 years and their AUCs.

(E and F) The calibration curve and DCA showed the predictive accuracy of the nomogram. (*p < 0.05, ***p < 0.001).

0.84, 0.80, and 0.71, respectively (Figure 5D). Furthermore, we performed the calibration curve and decision curve analysis (DCA) to evaluate the predictive accuracy (Figures 5E and 5F).

Functional enrichment analysis of the prognosis signature

The cellular zinc homeostasis was largely maintained by ZIP and ZnT zinc transporters. They are mostly located in the cell membrane; they indicate the potential function of absorbing and releasing zinc between cells and intercellular substance.[22] To explore potential zinc homeostasis status in different groups in TCGA cohort, we examined the corresponding mRNA levels of these transporters. The results showed that most ZIP transporters were upregulated in groups with the higher risk (Figure 6A). Gene set enrichment analysis (GSEA) was performed to assess the molecular mechanisms. In the group of patients with higher risk scores, cellular response to zinc ion and immune associated pathways were weakened, such as natural killer (NK) cell activation, neutrophil mediated cytotoxicity, regulation of dendritic cell differentiation, peptide antigen assembly with major histocompatibility complex (MHC) protein complex, CD4-positive alpha-beta T cell lineage commitment, and T-helper 2 cell cytokine production (Figures 6B and S2A–S2F). In contrast, cell proliferation and extracellular matrix (ECM) related

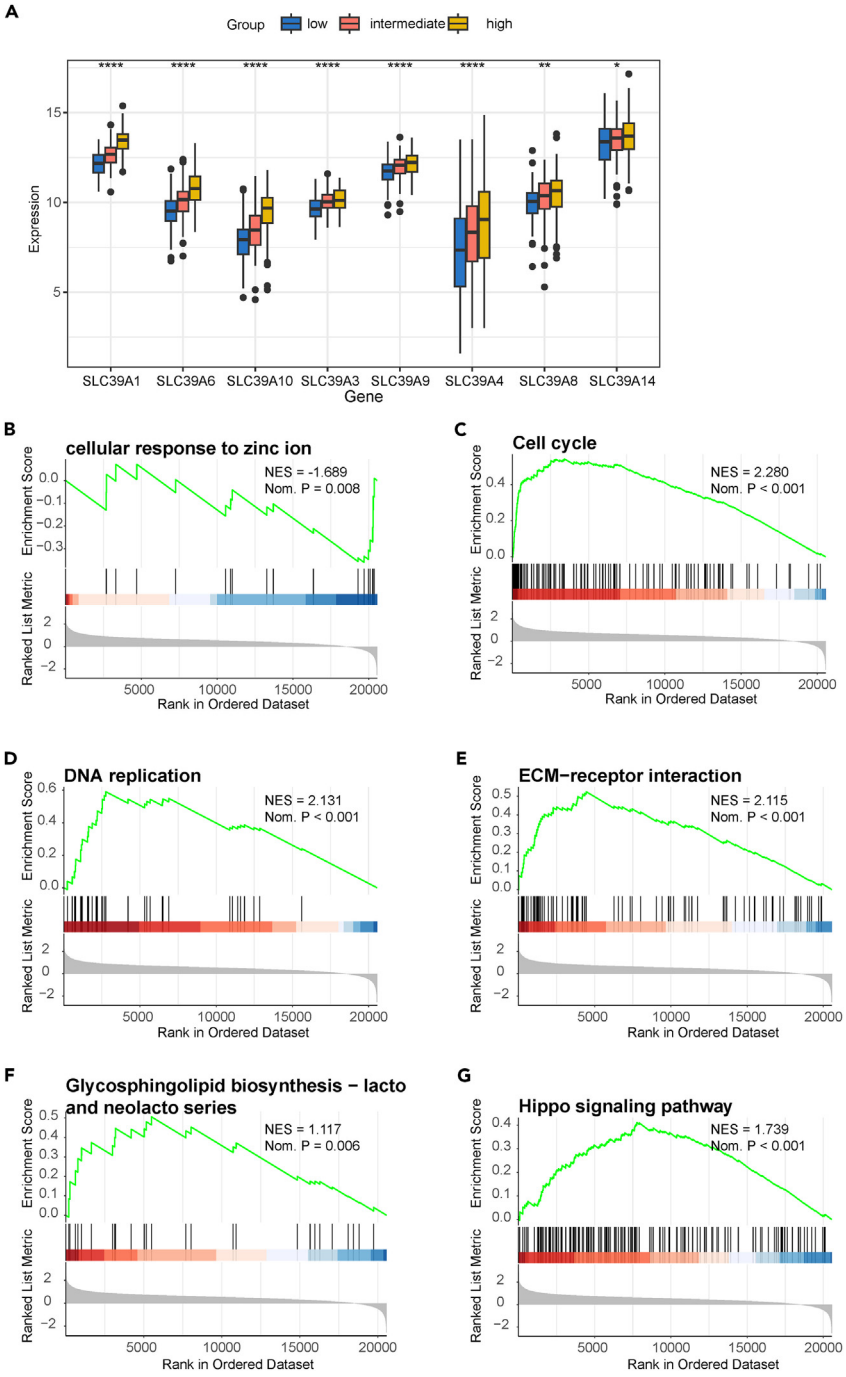

Figure 6. Functional enrichment analysis of the prognosis signature

(A) Expression of zinc homeostasis-related transporters in the TCGA cohort.

(B) GSEA showed that the pathway of cellular response to zinc ion was related to the lower-risk group based on the Gene Ontology (GO) biological processes.

(C–G) GSEA showed the significant enrichment of cell proliferation, ECM related pathways, and hippo signaling pathways in the higher-risk group based on the Kyoto Encyclopedia of Genes and Genomes (KEGG) pathways. (*p < 0.05, **p < 0.01, ****p < 0.0001).

pathways, including cell cycle, DNA replication, ECM-receptor interaction, and glycosphingolipid biosynthesis, were enriched (Figures 6C–6F, and S2G–S2I). Moreover, these patients were more relevant with the hippo signaling pathway (Figure 6G). The detail results of GESA analysis are presented in Tables S6 and S7.

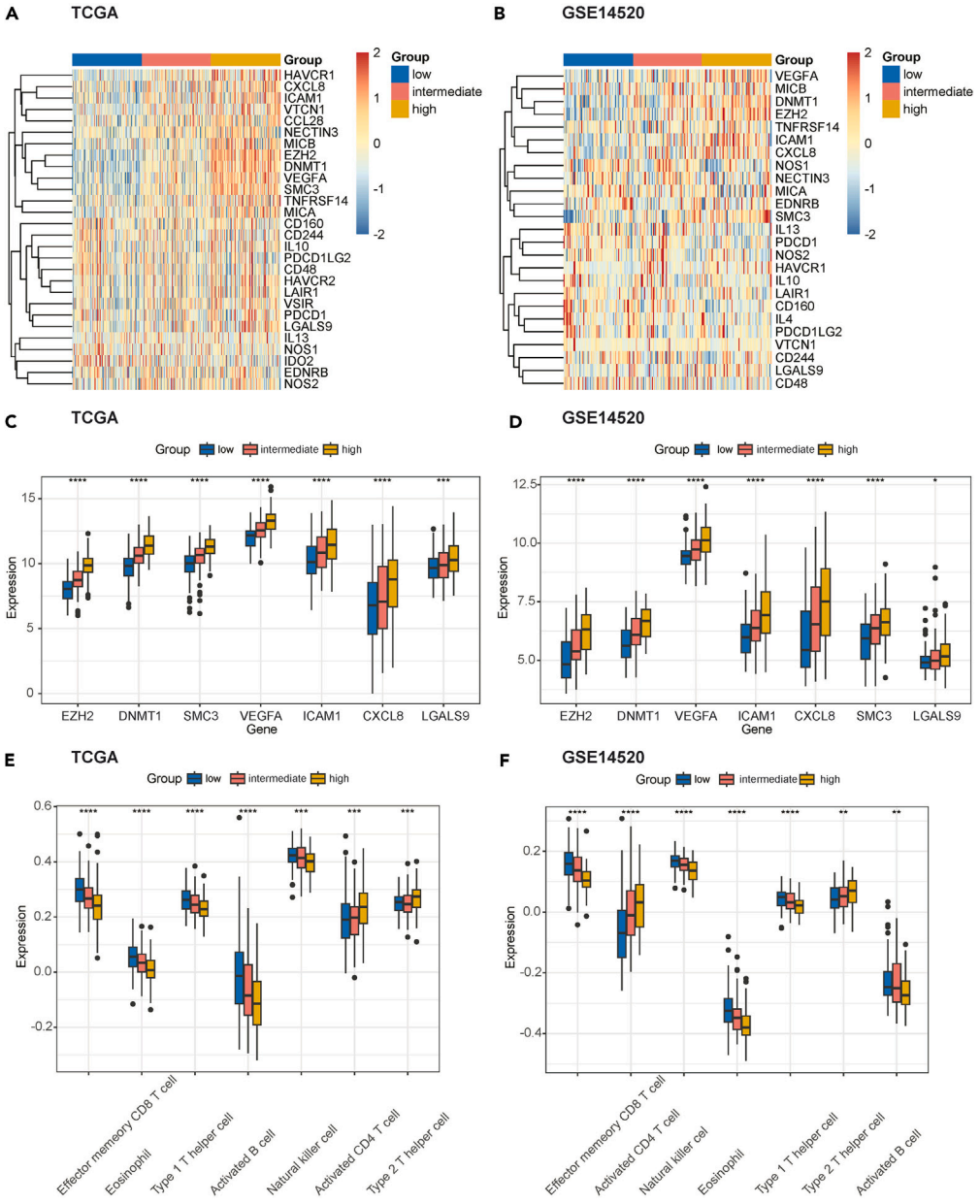

Figure 7. Immune features of zinc homeostasis-related prognosis signature

(A and B) Heatmap revealed the expression of cancer-related immunosuppressive genes in the low-, intermediate- and high-risk groups in the TCGA and GSE14520 cohorts.

(C and D) The expression of *CXCL8*, *DNMT1*, *EZH2*, *ICAM1*, *LGALS9*, *SMC3*, and *VEGFA* in different groups in the two cohorts.

(E and F) Relative tumor infiltrating immune cells with a remarkable difference in the low-, intermediate-, and high-risk groups in the two cohorts. (*$p < 0.05$, **$p < 0.01$, ***$p < 0.001$, ****$p < 0.0001$).

Immune features of zinc homeostasis-related prognosis signature

To explore the link between tumor immunity and the risk model, the expression of immunosuppressive genes[23] were examined in different risk groups in two cohorts and we found that most genes were upregulated when the risk increased (Figures 7A and 7B). *CXCL8*, *DNMT1*, *EZH2*, *ICAM1*, *LGALS9*, *SMC3*, and *VEGFA* were the identical immune characteristics positively related with the risk score (Figures 7C and 7D). We also found that most immune checkpoint genes were overexpressed in the groups with higher risk scores in TCGA cohort (Figure S3A). Based on the expression level and the zinc homeostasis-related risk score, *CD276*, *NRP1*, and *TNFSF4* were the top three genes highly relevant with the risk score (Figures S3B–S3E).

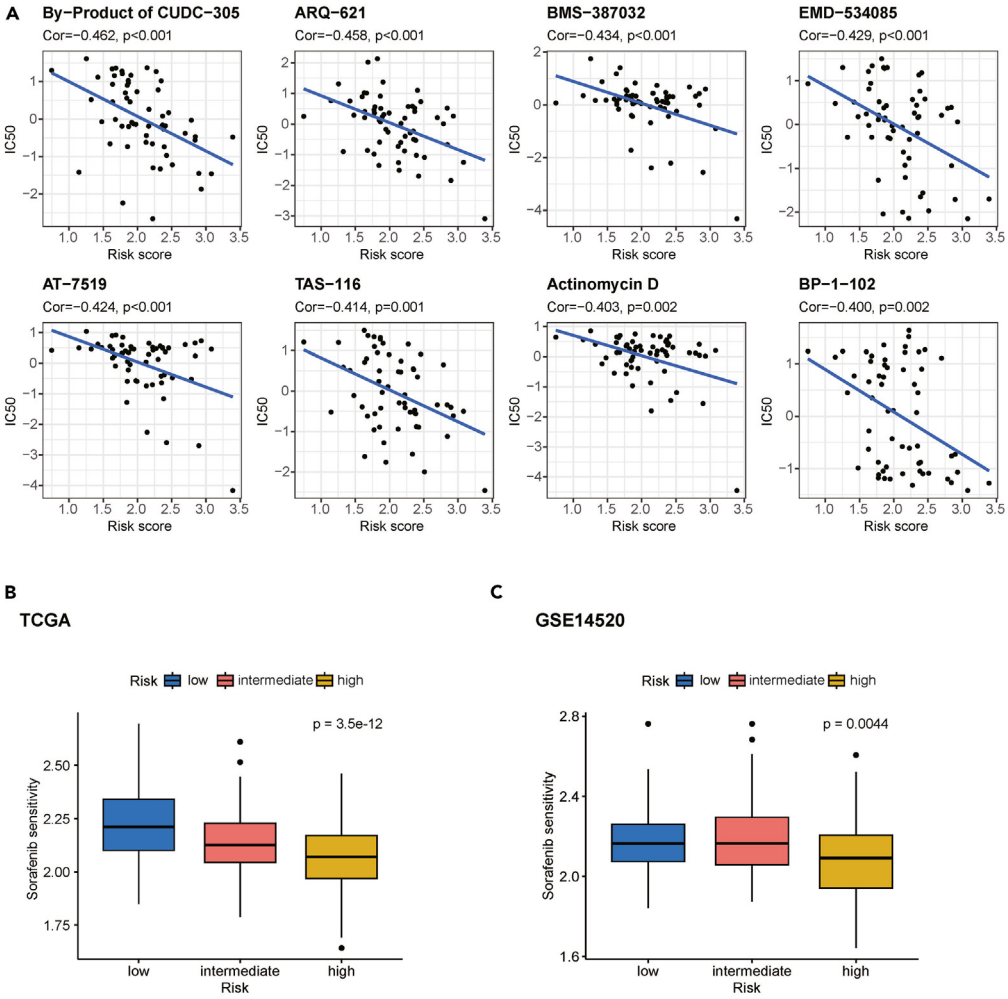

Figure 8. Higher-risk patients were more sensitive to sorafenib and other antitumor drugs

(A) CUDC-305, ARQ-621, BMS-387032, EMD-534085, AT-7519, TAS-116, actinomycin D, and BP-1-102 were negatively correlated with the risk score based on the CellMiner database.

(B and C) Drug sensitivity of sorafenib in the low-, intermediate-, and high-risk groups in the TCGA and GSE14520 cohorts.

The single sample Gene Set Enrichment Analysis (ssGSEA) method was applied to assess the immune cell distribution in two cohorts (Figures S4A and S4B). The results demonstrated that effector memory $CD8^+$ T cell, eosinophil, type 1 T helper (Th1) cell, NK cell, and activated B cell were decreased in the higher-risk groups. In contrast, activated $CD4^+$ T cell and type 2 T helper (Th2) cell were increased in both cohorts (Figures 7E and 7F).

Higher-risk patients were more sensitive to sorafenib and other antitumor drugs

To better understand the potential clinical application of the prognosis signature, CellMiner database was applied to analyze the relation of drug sensitivity and the risk score. Overall, 860 drugs approved by clinical trials or Food and Drug Administration (FDA) were chosen for analysis (Table S8). The risk score was negatively associated with the sensitivity of the by-product of CUDC-305, ARQ-621, BMS-387032, EMD-534085, AT-7519, TAS-116, actinomycin D, and BP-1-102 (Figure 8A). In addition, we utilized *pRRophitic* package to estimate the drug sensitivity difference in both cohorts and observed that sorafenib had a lower IC_{50} in higher-risk groups (Figures 8B and 8C). In this prognostic model, patients with higher risk scores were more sensitive to sorafenib and other clinical trials or FDA-approved drugs. The data of drug screening provided the support of the use of these drugs in the clinical treatment of higher-risk patients with HCC to promote their poor survival events.

DISCUSSION

Zinc homeostasis is an essential biological event in the human body and is strictly regulated by many proteins for maintaining the optimal systemic and cellular zinc level.[9] In these mediators, ZIP and ZnT transporters help in importing and storing zinc.[24] The dysfunction of zinc

homeostasis can affect the gene transcriptional regulation involved in cellular signaling, cell viability, proliferation, invasiveness, apoptosis, and metabolism in various cancers.[25–27] Regarding HCC, previous studies have repeatedly confirmed that the zinc level had significantly diminished in the HCC tissues compared with the adjacent normal tissues.[28,29] Zinc transporters affect carcinogenesis in HCC and zinc deficiency is correlated with early malignancy.[19,20,30] Moreover, zinc homeostasis is essential for the immune cell pathway[31] and contributes to a well-functioning immune defense in innate and acquired immune systems.[32] The liver has a special and complex immune landscape since its functions as a central immunological organ and this feature provides patients with HCC with possibilities of immunotherapy despite the limited objective response rate.[33] Currently, the significance of zinc homeostasis in tumor immunity of HCC remains unknown. Therefore, we established a zinc homeostasis-related risk model to predict the outcome and explored better therapeutic strategies in HCC.

In this article, we retrieved the zinc homeostasis-associated genes from the GeneCards database and subjected them to KM and univariate Cox regression analyses in TCGA and GSE14520 cohorts. There remained 185 intersection genes associated with survival status. Further LASSO regression and multivariate Cox regression analyses were applied to identify five signature genes, including *ADAMTS5*, *KLRB1*, *PLOD2*, *PTDSS2*, and *UCK2* to construct an optimal prognostic model. Among these genes, *UCK2* was upregulated in tumor samples in two cohorts. The expression of *UCK2* in HCC was confirmed and the results indicated that *UCK2* was overexpressed in the tumor groups compared with the normal cell or tissues. We also found that *UCK2* was associated with the proliferation and migration in the HCC cell line. It is reported that *UCK2* participates in cancer progression and metastasis[34] by inducing the activation of EGFR-AKT[35] and STAT3 signaling pathways in HCC.[36] Additionally, *PLOD2* has poor influence on the outcome of patients with HCC and was significantly correlated with tumor size and metastasis.[37] In a cohort study including 48 patients with HCC, the expression level of *ADAMTS5* was reported to reduce in HCC and *ADAMTS5* was found to function as an inhibitory factor of tumor angiogenesis and tube formations.[38] *KLRB1*, also known as *CD161*, is overexpressed in the $CD8^+$ T cells in the TME of HCC and induces the phenotype of low cytotoxicity and clonal expansion.[39] The role of *PTDSS2* in HCC has not been clarified.

Patients with higher-risk scores were likely to have a worse outcome. ROC curves demonstrated that our prognostic model had a great performance in predicting 1-, 3-, and 5-year OS for people with HCC in TCGA and GSE14520 cohorts. To fully explore the application of the risk signature, we constructed a nomogram consisting of the risk score, tumor stage, age, and TMB level. The ROC, calibration, and DCA curves demonstrated the outstanding predictive capacity of the model.

Furthermore, we investigated the potential mechanisms comprehensively using GSEA method. Functional analysis revealed that the mitosis and ECM-related pathways were enriched in patients with higher risk scores, demonstrating the connection between zinc homeostasis and tumor progression. Zinc affects mitosis[40] and zinc deficiency affects the zinc-dependent enzyme catalysis and intracellular signaling systems associated with cell proliferation.[41] Zinc also participates in cancer metastasis by modulating the downstream target protein *ZEB1*, thereby promoting the epithelial mesenchymal transition (EMT) plasticity in pancreatic[17] and breast cancers.[42] The results of GSEA demonstrated that multiple immune-related signaling pathways are more relevant with patients with lower-risk HCC, consisting of NK cell, neutrophil, dendritic cell, and T cell-associated immune activation and response, indicating that the dysfunction of zinc homeostasis may cause immune defense deficiency in the host. The cellular response to zinc ion was decreased while we surprisingly found that most ZIP transporters on the cell membrane were overexpressed in the higher-risk group. We hypothesized that it was partially due to the feedback regulation of the human body, considering that ZIP transporters would be induced to express more when the cell is deficient of zinc.[9] In addition, the expression level of most immunosuppressive genes was increased in the higher-risk group. Among them, *CXCL8*, *VEGFA*, and *DNMT1* can stimulate the angiogenesis and tumorigenesis of HCC.[43] *ICAM1* participates in efficient extravasation in HCC metastasis.[44] *EZH2* modulates the epigenetic modification of PD-L1 in HCC cell lines[45] and a recent research of the single-cell RNA sequencing analysis revealed that *LGALS9* is mainly expressed in tumor-associated macrophages and the encoding production is involved in immune escape.[46] *SMC3* is upregulated and associated with a poor outcome in HCC.[47] We also found that various immune checkpoints exhibited the higher expression levels in patients with higher-risk scores, implying these patients may be more sensitive to related immune checkpoint inhibitors, providing a selective treatment for people with HCC. Immune cells are vital elements in the TME and they participate in antitumor immunity and tumor immune evasion.[48] In this respect, the infiltrations of $CD8^+$ T cells, Th1 cells, B cells, NK cells, and eosinophils reduced while the composition of activated $CD4^+$ T cells and Th2 cells increased. Activated $CD4^+$ T cells can differentiate into several T cell phenotypes including Th1 and Th2 cells under the stimulation of cytokines. However, Th1 and Th2 cytokines play the opposite roles in pro- or anti-inflammatory processes in HCC. Th1 cytokines induce the activation and proliferation of $CD8^+$ T cells and NK cells, thus promote the anti-tumor immunity. Th2 cytokines can suppress the Th1 cell differentiation and active the immunosuppressive cells, such as myeloid-derived suppressor cells.[49] These evidences illustrated the critical connection between the risk signature and immune status in HCC, indicating that the higher-risk patients may benefit more from tumor immunotherapies.

Furthermore, eight drugs approved by the clinical trials or FDA were filtered. Recently, BMS-387032 (also known as SNS-023) was found to induce apoptosis and suppress the cell proliferation and migration by targeting the EGFR-AKT pathway in HCC. In addition, the drug combination of BMS-387032 and sorafenib showed the powerful synergistic effect on inhibiting HCC xenografts *in vivo*.[50] Another research declaimed the actinomycin had the selective capacity to inhibit liver cancer stem cells.[51] In addition, the higher-risk patients were more sensitive to sorafenib, the FDA-approved drug for patients with advanced HCC since 2007 as a tyrosine kinase inhibitor,[52] and the development of resistance to sorafenib has become a great challenge.[53] Therefore, our prognostic model suggested that these drugs with higher sensitivity may be more effective for the higher-risk patients with HCC and rescue their prognosis in the clinical treatment.

In summary, we established a prognostic model by elucidating the specific role of zinc homeostasis in HCC and proposed a potential therapeutic strategy for HCC.

Limitations of the study

As for limitations, the construction and validation of this zinc homeostasis-related risk model were based on two public cohorts of people with HCC. In the subsequent work, we will conduct clinical trials for patients with HCC to evaluate the abilities in predicting prognostic outcomes and drug response effects based on our risk model. Also, it may be not considerate enough that patients were simply divided into three groups, considering the current clinical groups of HCC. More analyses should be carried out to make the risk model more precise in the future work. In this study, we screened out five signature genes and found that *UCK2* participated in proliferation and migration of HCC. More surveys will be carried out to investigate the potential function of five signatures genes in HCC progression. The molecular mechanisms of these genes in regulating immune microenvironment and drug sensitivity are needed to be clarified further by experimental supports.

STAR★METHODS

Detailed methods are provided in the online version of this paper and include the following:

- KEY RESOURCES TABLE
- RESOURCE AVAILABILITY
  - Lead contact
  - Materials availability
  - Data and code availability
- EXPERIMENTAL MODEL AND STUDY PARTICIPANT DETAILS
  - Patient recruitment & sample acquisition
  - Cell lines
- METHOD DETAILS
  - Data acquisition
  - Construction, validation and evaluation of the prognostic signature
  - Construction and evaluation of the nomogram
  - Function enrichment analysis and immunocyte infiltration analysis
  - Drug sensitivity based on the prognosis signature
  - Western blotting
  - RNA extraction and quantitative real-time PCR
  - Immunohistochemistry
  - Small interfering RNA (siRNA) interference
  - Clone formation assay and CCK-8 assay
  - Wound healing assay and cell migration assay
- QUANTIFICATION AND STATISTICAL ANALYSIS

SUPPLEMENTAL INFORMATION

Supplemental information can be found online at https://doi.org/10.1016/j.isci.2024.109389.

ACKNOWLEDGMENTS

This work was supported, in part, by the National Natural Science Foundation of China (numbers 92169203, 31970151, 82102384, 82172239, 82271778, and 32041006), the National Natural Science Foundation of Zhejiang Province (LQ21C010001 and LY22C080002), and the Leading innovative and Entrepreneur Team Introduction Program of Zhejiang (2019R01007).

AUTHOR CONTRIBUTIONS

Y.S. and R.Y. contributed equally to this work. All authors had read and commented on the manuscript, gave final approval, and agreed to be accountable for all aspects of work ensuring integrity and accuracy.

Y.S.: data curation, project administration, writing – review & editing. R.Y.: data curation, project administration, writing – review & editing. Y.G.: formal analysis and writing – original draft. F.X.: formal analysis. X.-F.Y.: data curation, project administration, writing – review & editing, funding acquisition, and supervision.

DECLARATION OF INTERESTS

The authors declare no conflicts of interests.

Received: September 12, 2023
Revised: January 15, 2024
Accepted: February 28, 2024
Published: March 2, 2024

REFERENCES

1. Siegel, R.L., Miller, K.D., Fuchs, H.E., and Jemal, A. (2022). Cancer statistics, 2022. CA. Cancer J. Clin. *72*, 7–33. https://doi.org/10.3322/caac.21708.
2. Llovet, J.M., Kelley, R.K., Villanueva, A., Singal, A.G., Pikarsky, E., Roayaie, S., Lencioni, R., Koike, K., Zucman-Rossi, J., and Finn, R.S. (2021). Hepatocellular carcinoma. Nat. Rev. Dis. Prim. *7*, 6. https://doi.org/10.1038/s41572-020-00240-3.
3. Schulze, K., Nault, J.C., and Villanueva, A. (2016). Genetic profiling of hepatocellular carcinoma using next-generation sequencing. J. Hepatol. *65*, 1031–1042. https://doi.org/10.1016/j.jhep.2016.05.035.
4. Vogel, A., Meyer, T., Sapisochin, G., Salem, R., and Saborowski, A. (2022). Hepatocellular carcinoma. Lancet *400*, 1345–1362. https://doi.org/10.1016/s0140-6736(22)01200-4.
5. Tabrizian, P., Jibara, G., Shrager, B., Schwartz, M., and Roayaie, S. (2015). Recurrence of hepatocellular cancer after resection: patterns, treatments, and prognosis. Ann. Surg. *261*, 947–955. https://doi.org/10.1097/sla.0000000000000710.
6. Greten, T.F., Villanueva, A., Korangy, F., Ruf, B., Yarchoan, M., Ma, L., Ruppin, E., and Wang, X.W. (2023). Biomarkers for immunotherapy of hepatocellular carcinoma. Nat. Rev. Clin. Oncol. *20*, 780–798. https://doi.org/10.1038/s41571-023-00816-4.
7. Yang, C., Zhang, H., Zhang, L., Zhu, A.X., Bernards, R., Qin, W., and Wang, C. (2023). Evolving therapeutic landscape of advanced hepatocellular carcinoma. Nat. Rev. Gastroenterol. Hepatol. *20*, 203–222. https://doi.org/10.1038/s41575-022-00704-9.
8. Kolenko, V., Teper, E., Kutikov, A., and Uzzo, R. (2013). Zinc and zinc transporters in prostate carcinogenesis. Nat. Rev. Urol. *10*, 219–226. https://doi.org/10.1038/nrurol.2013.43.
9. Kambe, T., Tsuji, T., Hashimoto, A., and Itsumura, N. (2015). The Physiological, Biochemical, and Molecular Roles of Zinc Transporters in Zinc Homeostasis and Metabolism. Physiol. Rev. *95*, 749–784. https://doi.org/10.1152/physrev.00035.2014.
10. Murakami, M., and Hirano, T. (2008). Intracellular zinc homeostasis and zinc signaling. Cancer Sci. *99*, 1515–1522. https://doi.org/10.1111/j.1349-7006.2008.00854.x.
11. Prasad, A.S. (1985). Clinical manifestations of zinc deficiency. Annu. Rev. Nutr. *5*, 341–363. https://doi.org/10.1146/annurev.nu.05.070185.002013.
12. Sensi, S.L., Granzotto, A., Siotto, M., and Squitti, R. (2018). Copper and Zinc Dysregulation in Alzheimer's Disease. Trends Pharmacol. Sci. *39*, 1049–1063. https://doi.org/10.1016/j.tips.2018.10.001.
13. Duce, J.A., Tsatsanis, A., Cater, M.A., James, S.A., Robb, E., Wikhe, K., Leong, S.L., Perez, K., Johanssen, T., Greenough, M.A., et al. (2010). Iron-export ferroxidase activity of β-amyloid precursor protein is inhibited by zinc in Alzheimer's disease. Cell *142*, 857–867. https://doi.org/10.1016/j.cell.2010.08.014.
14. Prasad, A.S., and Cossack, Z.T. (1984). Zinc supplementation and growth in sickle cell disease. Ann. Intern. Med. *100*, 367–371. https://doi.org/10.7326/0003-4819-100-3-367.
15. Costello, L.C., and Franklin, R.B. (2017). Decreased zinc in the development and progression of malignancy: an important common relationship and potential for prevention and treatment of carcinomas. Expert Opin. Ther. Targets *21*, 51–66. https://doi.org/10.1080/14728222.2017.1265506.
16. Franklin, R.B., Feng, P., Milon, B., Desouki, M.M., Singh, K.K., Kajdacsy-Balla, A., Bagasra, O., and Costello, L.C. (2005). hZIP1 zinc uptake transporter down regulation and zinc depletion in prostate cancer. Mol. Cancer *4*, 32. https://doi.org/10.1186/1476-4598-4-32.
17. Liu, M., Zhang, Y., Yang, J., Zhan, H., Zhou, Z., Jiang, Y., Shi, X., Fan, X., Zhang, J., Luo, W., et al. (2021). Zinc-Dependent Regulation of ZEB1 and YAP1 Coactivation Promotes Epithelial-Mesenchymal Transition Plasticity and Metastasis in Pancreatic Cancer. Gastroenterology *160*, 1771–1783.e1. https://doi.org/10.1053/j.gastro.2020.12.077.
18. Chandler, P., Kochupurakkal, B.S., Alam, S., Richardson, A.L., Soybel, D.I., and Kelleher, S.L. (2016). Subtype-specific accumulation of intracellular zinc pools is associated with the malignant phenotype in breast cancer. Mol. Cancer *15*, 2. https://doi.org/10.1186/s12943-015-0486-y.
19. Xu, X., Guo, H.J., Xie, H.Y., Li, J., Zhuang, R.Z., Ling, Q., Zhou, L., Wei, X.Y., Liu, Z.K., Ding, S.M., et al. (2014). ZIP4, a novel determinant of tumor invasion in hepatocellular carcinoma, contributes to tumor recurrence after liver transplantation. Int. J. Biol. Sci. *10*, 245–256. https://doi.org/10.7150/ijbs.7401.
20. Costello, L.C., and Franklin, R.B. (2014). The status of zinc in the development of hepatocellular cancer: an important, but neglected, clinically established relationship. Cancer Biol. Ther. *15*, 353–360. https://doi.org/10.4161/cbt.27633.
21. Cen, D., Ge, Q., Xie, C., Zheng, Q., Guo, J., Zhang, Y., Wang, Y., Li, X., Gu, Z., and Cai, X. (2021). ZnS@BSA Nanoclusters Potentiate Efficacy of Cancer Immunotherapy. Adv. Mater. *33*, e2104037. https://doi.org/10.1002/adma.202104037.
22. Kambe, T., Taylor, K.M., and Fu, D. (2021). Zinc transporters and their functional integration in mammalian cells. J. Biol. Chem. *296*, 100320. https://doi.org/10.1016/j.jbc.2021.100320.
23. Xu, L., Deng, C., Pang, B., Zhang, X., Liu, W., Liao, G., Yuan, H., Cheng, P., Li, F., Long, Z., et al. (2018). TIP: A Web Server for Resolving Tumor Immunophenotype Profiling. Cancer Res. *78*, 6575–6580. https://doi.org/10.1158/0008-5472.Can-18-0689.
24. Lichten, L.A., and Cousins, R.J. (2009). Mammalian zinc transporters: nutritional and physiologic regulation. Annu. Rev. Nutr. *29*, 153–176. https://doi.org/10.1146/annurev-nutr-033009-083312.
25. Xiao, W., Wang, J., Wang, X., Cai, S., Guo, Y., Ye, L., Li, D., Hu, A., Jin, S., Yuan, B., et al. (2022). Therapeutic targeting of the USP2-E2F4 axis inhibits autophagic machinery essential for zinc homeostasis in cancer progression. Autophagy *18*, 2615–2635. https://doi.org/10.1080/15548627.2022.2044651.
26. Lv, M., Cao, D., Zhang, L., Hu, C., Li, S., Zhang, P., Zhu, L., Yi, X., Li, C., Yang, A., et al. (2021). METTL9 mediated N1-histidine methylation of zinc transporters is required for tumor growth. Protein Cell *12*, 965–970. https://doi.org/10.1007/s13238-021-00857-4.
27. Costello, L.C., and Franklin, R.B. (2006). The clinical relevance of the metabolism of prostate cancer; zinc and tumor suppression: connecting the dots. Mol. Cancer *5*, 17. https://doi.org/10.1186/1476-4598-5-17.
28. Ebara, M., Fukuda, H., Hatano, R., Saisho, H., Nagato, Y., Suzuki, K., Nakajima, K., Yukawa, M., Kondo, F., Nakayama, A., and Sakurai, H. (2000). Relationship between copper, zinc and metallothionein in hepatocellular carcinoma and its surrounding liver parenchyma. J. Hepatol. *33*, 415–422. https://doi.org/10.1016/s0168-8278(00)80277-9.
29. Tashiro, H., Kawamoto, T., Okubo, T., and Koide, O. (2003). Variation in the distribution of trace elements in hepatoma. Biol. Trace Elem. Res. *95*, 49–63. https://doi.org/10.1385/bter:95:1:49.
30. Gartmann, L., Wex, T., Grüngreiff, K., Reinhold, D., Kalinski, T., Malfertheiner, P., and Schütte, K. (2018). Expression of zinc transporters ZIP4, ZIP14 and ZnT9 in hepatic carcinogenesis-An immunohistochemical study. J. Trace Elem. Med. Biol. *49*, 35–42. https://doi.org/10.1016/j.jtemb.2018.04.034.
31. Kim, B., and Lee, W.W. (2021). Regulatory Role of Zinc in Immune Cell Signaling. Mol. Cell. *44*, 335–341. https://doi.org/10.14348/molcells.2021.0061.
32. Maywald, M., and Rink, L. (2022). Zinc in Human Health and Infectious Diseases. Biomolecules *12*, 1748. https://doi.org/10.3390/biom12121748.
33. Ruf, B., Heinrich, B., and Greten, T.F. (2021). Immunobiology and immunotherapy of HCC: spotlight on innate and innate-like immune cells. Cell. Mol. Immunol. *18*, 112–127. https://doi.org/10.1038/s41423-020-00572-w.
34. Yu, Y., You, S., Fan, R., and Shan, X. (2022). UCK2 regulated by miR-139-3p regulates the progression of hepatocellular carcinoma cells. Future Oncol. *18*, 979–990. https://doi.org/10.2217/fon-2021-0271.
35. Cai, J., Sun, X., Guo, H., Qu, X., Huang, H., Yu, C., Wu, H., Gao, Y., Kong, X., and Xia, Q. (2020). Non-metabolic role of UCK2 links EGFR-AKT pathway activation to metastasis enhancement in hepatocellular carcinoma. Oncogenesis *9*, 103. https://doi.org/10.1038/s41389-020-00287-7.
36. Zhou, Q., Jiang, H., Zhang, J., Yu, W., Zhou, Z., Huang, P., Wang, J., and Xiao, Z. (2018). Uridine-cytidine kinase 2 promotes metastasis of hepatocellular carcinoma cells

via the Stat3 pathway. Cancer Manag. Res. *10*, 6339–6355. https://doi.org/10.2147/cmar.S182859.

37. Noda, T., Yamamoto, H., Takemasa, I., Yamada, D., Uemura, M., Wada, H., Kobayashi, S., Marubashi, S., Eguchi, H., Tanemura, M., et al. (2012). PLOD2 induced under hypoxia is a novel prognostic factor for hepatocellular carcinoma after curative resection. Liver Int. *32*, 110–118. https://doi.org/10.1111/j.1478-3231.2011.02619.x.
38. Li, C., Xiong, Y., Yang, X., Wang, L., Zhang, S., Dai, N., Li, M., Ren, T., Yang, Y., Zhou, S.F., et al. (2015). Lost expression of ADAMTS5 protein associates with progression and poor prognosis of hepatocellular carcinoma. Drug Des. Dev. Ther. *9*, 1773–1783. https://doi.org/10.2147/dddt.S77069.
39. Sun, Y., Wu, L., Zhong, Y., Zhou, K., Hou, Y., Wang, Z., Zhang, Z., Xie, J., Wang, C., Chen, D., et al. (2021). Single-cell landscape of the ecosystem in early-relapse hepatocellular carcinoma. Cell *184*, 404–421.e16. https://doi.org/10.1016/j.cell.2020.11.041.
40. Fujii, T. (1954). Presence of zinc in nucleoli and its possible role in mitosis. Nature *174*, 1108–1109. https://doi.org/10.1038/1741108a0.
41. MacDonald, R.S. (2000). The role of zinc in growth and cell proliferation. J. Nutr. *130*, 1500s-8S. https://doi.org/10.1093/jn/130.5.1500S.
42. Mohammadi Ghahhari, N., Sznurkowska, M.K., Hulo, N., Bernasconi, L., Aceto, N., and Picard, D. (2022). Cooperative interaction between ERα and the EMT-inducer ZEB1 reprograms breast cancer cells for bone metastasis. Nat. Commun. *13*, 2104. https://doi.org/10.1038/s41467-022-29723-5.
43. Wang, Q., Liang, N., Yang, T., Li, Y., Li, J., Huang, Q., Wu, C., Sun, L., Zhou, X., Cheng, X., et al. (2021). DNMT1-mediated methylation of BEX1 regulates stemness and tumorigenicity in liver cancer. J. Hepatol. *75*, 1142–1153. https://doi.org/10.1016/j.jhep.2021.06.025.
44. Brodt, P. (2016). Role of the Microenvironment in Liver Metastasis: From Pre- to Prometastatic Niches. Clin. Cancer Res. *22*, 5971–5982. https://doi.org/10.1158/1078-0432.Ccr-16-0460.
45. Xiao, G., Jin, L.L., Liu, C.Q., Wang, Y.C., Meng, Y.M., Zhou, Z.G., Chen, J., Yu, X.J., Zhang, Y.J., Xu, J., and Zheng, L. (2019). EZH2 negatively regulates PD-L1 expression in hepatocellular carcinoma. J. Immunother. Cancer *7*, 300. https://doi.org/10.1186/s40425-019-0784-9.
46. Ma, L., Heinrich, S., Wang, L., Keggenhoff, F.L., Khatib, S., Forgues, M., Kelly, M., Hewitt, S.M., Saif, A., Hernandez, J.M., et al. (2022). Multiregional single-cell dissection of tumor and immune cells reveals stable lock-and-key features in liver cancer. Nat. Commun. *13*, 7533. https://doi.org/10.1038/s41467-022-35291-5.
47. Yan, W., Wang, D.D., Zhang, H.D., Huang, J., Hou, J.C., Yang, S.J., Zhang, J., Lu, L., and Zhang, Q. (2022). Expression profile and prognostic values of SMC family members in HCC. Medicine *101*, e31336. https://doi.org/10.1097/md.0000000000031336.
48. Quail, D.F., and Joyce, J.A. (2013). Microenvironmental regulation of tumor progression and metastasis. Nat. Med. *19*, 1423–1437. https://doi.org/10.1038/nm.3394.
49. Budhu, A., and Wang, X.W. (2006). The role of cytokines in hepatocellular carcinoma. J. Leukoc. Biol. *80*, 1197–1213. https://doi.org/10.1189/jlb.0506297.
50. Liu, Y., Kong, W.Y., Yu, C.F., Shao, Z.L., Lei, Q.C., Deng, Y.F., Cai, G.X., Zhuang, X.F., Sun, W.S., Wu, S.G., et al. (2023). SNS-023 sensitizes hepatocellular carcinoma to sorafenib by inducing degradation of cancer drivers SIX1 and RPS16. Acta Pharmacol. Sin. *44*, 853–864. https://doi.org/10.1038/s41401-022-01003-4.
51. Song, Y., Park, I.S., Kim, J., and Seo, H.R. (2019). Actinomycin D inhibits the expression of the cystine/glutamate transporter xCT via attenuation of CD133 synthesis in CD133(+) HCC. Chem. Biol. Interact. *309*, 108713. https://doi.org/10.1016/j.cbi.2019.06.026.
52. Foerster, F., Gairing, S.J., Ilyas, S.I., and Galle, P.R. (2022). Emerging immunotherapy for HCC: A guide for hepatologists. Hepatology *75*, 1604–1626. https://doi.org/10.1002/hep.32447.
53. Tang, W., Chen, Z., Zhang, W., Cheng, Y., Zhang, B., Wu, F., Wang, Q., Wang, S., Rong, D., Reiter, F.P., et al. (2020). The mechanisms of sorafenib resistance in hepatocellular carcinoma: theoretical basis and therapeutic aspects. Signal Transduct. Targeted Ther. *5*, 87. https://doi.org/10.1038/s41392-020-0187-x.
54. Colaprico, A., Silva, T.C., Olsen, C., Garofano, L., Cava, C., Garolini, D., Sabedot, T.S., Malta, T.M., Pagnotta, S.M., Castiglioni, I., et al. (2016). TCGAbiolinks: an R/Bioconductor package for integrative analysis of TCGA data. Nucleic Acids Res. *44*, e71. https://doi.org/10.1093/nar/gkv1507.
55. Roessler, S., Jia, H.L., Budhu, A., Forgues, M., Ye, Q.H., Lee, J.S., Thorgeirsson, S.S., Sun, Z., Tang, Z.Y., Qin, L.X., and Wang, X.W. (2010). A unique metastasis gene signature enables prediction of tumor relapse in early-stage hepatocellular carcinoma patients. Cancer Res. *70*, 10202–10212. https://doi.org/10.1158/0008-5472.Can-10-2607.
56. Blanche, P., Dartigues, J.F., and Jacqmin-Gadda, H. (2013). Estimating and comparing time-dependent areas under receiver operating characteristic curves for censored event times with competing risks. Stat. Med. *32*, 5381–5397. https://doi.org/10.1002/sim.5958.
57. Charoentong, P., Finotello, F., Angelova, M., Mayer, C., Efremova, M., Rieder, D., Hackl, H., and Trajanoski, Z. (2017). Pan-cancer Immunogenomic Analyses Reveal Genotype-Immunophenotype Relationships and Predictors of Response to Checkpoint Blockade. Cell Rep. *18*, 248–262. https://doi.org/10.1016/j.celrep.2016.12.019.

STAR★METHODS

KEY RESOURCES TABLE

REAGENT or RESOURCE	SOURCE	IDENTIFIER
Antibodies		
Rabbit Polyclonal anti-GAPDH	Proteintech	Cat#10494-1-AP; RRID: AB_2651132
Rabbit Polyclonal anti-UCK2	Proteintech	Cat#10511-1-AP; RRID: AB_2048657
Biological samples		
HCC patient tumor tissues	Cancer Institute, The Second Affiliated Hospital, School of Medicine, Zhejiang University	N/A
Chemicals, peptides, and recombinant proteins		
Radioimmunoprecipitation assay lysis buffer	YEASEN	Cat#20114ES60
5 X loading buffer	Beyotime	Cat#P0015L
Enhanced chemiluminescence Substrate	Proteintech	Cat#PK10002
AG RNAex Pro Reagent	Accurate Biology	Cat#AG21102
RNAiMAX	Invitrogen	Cat#13778-150
Critical commercial assays		
CCK-8 kit	Beyotime	Cat#C0038
Eco M-MLV RT Premix kit	Accurate Biology	Cat#AG11706
SYBR Green Pro Taq HS kit	Accurate Biology	Cat#AG11701
Deposited data		
Processed microarray data and information of TCGA HCC samples	Colaprico et al.[54]	www.cancer.gov/tcga
Processed microarray data of human HCC	Roessler et al.[55]	GEO: GSE14520
Experimental models: Cell lines		
Human: HA22T	Laboratory of Hui Lin	RRID: CVCL_7046
Human: MIHA	Laboratory of Hui Lin	RRID: CVCL_SA11
Human: SMMC-7721	Laboratory of Hui Lin	RRID: CVCL_0336
Human: SK-HEP-1	ATCC	Cat#HTB-52
Human: SNU-449	ATCC	Cat#CRL-2234
Software and algorithms		
R (version 4.1.0)	N/A	N/A
GraphPad Prism software (version 8.0)	N/A	N/A
pRRophitic	R package	N/A
TCGAbiolinks	R package	N/A
Survival	R package	N/A
survminer	R package	N/A
limma	R package	N/A
tinyarray	R package	N/A
timeROC	R package	N/A
clusterProfiler	R package	N/A
GSVA	R package	N/A

RESOURCE AVAILABILITY

Lead contact

Further information and requests for resources should be directed and will be fulfilled by the lead contact, Xiao-Fang Yu (xfyu1@zju.edu.cn).

Materials availability

This study did not generate unique reagents.

Data and code availability

- This paper analyzed existing, publicly available data. These accession numbers for the datasets are also listed in the key resources table.
- This paper does no report original code.
- Any additional information required to reanalyze the data reported in this paper is available from the lead contact upon request.

EXPERIMENTAL MODEL AND STUDY PARTICIPANT DETAILS

Patient recruitment & sample acquisition

The RNA-seq data and clinical characteristics of human samples in this study were obtained from the Cancer Genome Atlas (TCGA) and gene expression omnibus (GEO) databases. The clinical information of patients for experimental researches was shown in Table S9. All patients provided written informed, and all samples were obtained upon approval of the Ethics Committee of the Second Affiliated Hospital of Zhejiang University, with the approval number 2023-0570.

Cell lines

The normal liver cell MIHA and HCC cell lines including SMMC-7721 and HA22Twere kindly provided by Professor Hui Lin (Department of General Surgery, Sir Run Run Shaw Hospital, School of Medicine, Zhejiang University). SK-HEP-1 (ATCC, Cat#HTB-52), SNU-449 (ATCC, Cat#CRL-2234), HA22T, MIHA, and SMMC-7721 were cultured in Dulbecco's modified Eagle's medium (Gibco, Cat#11965092) with 10% fetal bovine serum (FBS) (Gibco, Cat#12483020) and were cultured in the incubator containing 5% CO_2 at 37°C.

METHOD DETAILS

Data acquisition

The RNA sequencing (RNA-seq) transcriptome data and clinical information of The Cancer Genome Atlas (TCGA) (www.cancer.gov/tcga) were retrieved using *TCGAbiolinks* R package,[54] including 50 normal samples and 374 tumor samples among which 368 patients had complete clinical and prognostic data. The GES14520 cohort was acquired from Gene Expression Omnibus (GEO) database (https://www.ncbi.nlm.nih.gov/geo/),[55] including 220 normal samples and 225 tumor samples among which 209 patients had corresponding survival data. Patients with unknown survival information and genes expressed in less than half of tumor samples were filtered out. The detail clinical characteristics of patients in two cohorts were shown in Tables S1 and S2. We acquired zinc homeostasis-related genes from GeneCards (https://www.genecards.org/) and these genes are presented in Table S3.

Construction, validation and evaluation of the prognostic signature

The prognostic signature was constructed using the TCGA cohort as the training cohort and validated in the GSE14520 cohort. The OS-associated genes were obtained by univariate Cox regression and KM analyses by *survival* R package in two cohorts. P value < 0.05 in two methods simultaneously was defined as the screening criteria. LASSO regression and multivariate Cox regression analysis based on Akaike information criterion method were utilized to establish the optimal prognostic model. The risk score was calculated by the formula: Risk score = $\sum_{i=1}^{n}(Coef_i \times Exp_i)$, in which $Coef_i$ is the coefficient value and Exp_i represents the expression value of corresponding genes. The differential gene expression analysis was performed using *limma* package with the criteria of $p < 0.05$ and |Fold change (FC)| > 2.

The KM curves demonstrated the difference of OS using *survival* and *survminer* packages. The time-dependent ROC curves were performed to evaluate the sensitivity and specificity of the risk signature using *timeROC* package.[56] The AUC represented the predictive accuracy of the model. Furthermore, we utilized *tinyarray* package to perform a risk plot to reveal the distribution of survival situation and gene expression level.

Construction and evaluation of the nomogram

More clinical characteristics according to univariate and multivariate Cox regression analyses are illustrated in the form of forest plots. A nomogram was constructed in the TCGA cohort containing stage, TMB, age, and the risk score to display a personalized model. Calibration plots and DCA were performed to assess the predictive accuracy.

Function enrichment analysis and immunocyte infiltration analysis

We applied GSEA to explore the molecular mechanism in the Kyoto Encyclopedia of Genes and Genomes (KEGG) pathways and the Gene Ontology (GO) biological processes using *clusterProfiler* R package. Nominal $p < 0.05$, |Normalized Enrichment Score| > 1 and false discovery rate (FDR) < 0.25 were defined as the screening standard. Immunocyte infiltration degrees regarding 28 immunocyte subtypes in the TME were evaluated by *GSVA* package in R.[57]

Drug sensitivity based on the prognosis signature

We obtained the NCI-60 drug activity data and the transcriptome data from CellMiner database (https://discover.nci.nih.gov/cellminer/) to screen potential drugs whose half-maximal inhibitory concentrations (IC_{50}) were negatively associated with the risk score. The pRRophitic package (https://github.com/paulgeeleher/pRRophetic/) was used to predict the drug sensitivity difference between different groups in the TCGA and GSE14520 cohorts.

Western blotting

The cell samples were harvested and lysed using radioimmunoprecipitation assay lysis buffer (YEASEN, Cat#20114ES60) at 4°C for 20 min, mixed into 5 X loading buffer (Beyotime, Cat#P0015L), and boiled for 15 min. The protein was separated by sodium dodecyl sulfate-polyacrylamide gel electrophoresis gels and transferred to polyvinylidene fluoride membranes (0.45 um, Millipore) at 230 mA for 90 min. The membranes were blocked by 5% milk powder and incubated with primary antibodies against *GAPDH* (Proteintech, Cat#10494-1-AP) and *UCK2* (Proteintech, Cat#10511-1-AP) at 4°C overnight, followed by secondary antibodies. The blots were detected by enhanced chemiluminescence Substrate (Proteintech, Cat#PK10002) and detection system (Azure Biosystems). The quantification of protein band intensity was measured using ImageJ software (National Institutes of Health).

RNA extraction and quantitative real-time PCR

Total RNA was extracted using AG RNAex Pro Reagent (Accurate Biology, Cat#AG21102) following the manufacturer's protocol. The RNA was reverse-transcribed using Eco M-MLV RT Premix kit (Accurate Biology, Cat#AG11706) and the quantification of RNA was detected using SYBR Green Pro Taq HS kit (Accurate Biology, Cat#AG11701). We performed the reactions on the Roche LightCycler 480II PCR instrument (Basel, Switzerland). The primer sequences are as follows:

GAPDH: forward primer (5'-GGAGCGAGATCCCTCCAAAAT-3') and reverse primer (5'-GGCTGTTGTCATACTTCTCATGG-3');
UCK2: forward primer (5'-AGATCCCCGTGTATGACTTTGT-3') and reverse primer (5'-GGCTTGACGAACGTAATGTACTG-3').

Immunohistochemistry

The formalin-fixed paraffin-sealed tissues sections were dried in the incubator at 59°C for 60 min. The tissues were rehydrated three times for 10 min each in xylene, immersed in absolute ethanol three times, and washed with distilled water. The slides were then coated with the antigen retrieval solution, heated in the microwave oven over medium-high fire twice, and washed in phosphate buffered saline (PBS) twice for 15 min. In addition, 5% bovine serum albumin was added to the slides for 35 min and covered with the primary antibody using the dilution ratio of 1:50 at 4°C overnight, followed by the secondary antibody at 37°C for 35 min. The slides were coated with chromogenic solution, washed in water, stained with hematoxylin, and dehydrated in absolute ethanol and xylene. Finally, we sealed and observed the slides under the microscope. Visiopharm software was used to analyze the staining status and histochemistry score (H-score) was used to evaluate the relative staining intensity as follows: H-score = percentage of weak intensity X 1 + percentage of moderate intensity X 2 + percentage of strong intensity X 3.

Small interfering RNA (siRNA) interference

UCK2 siRNA (RiboBio, Cat#stB0003335A-1-5) and scrambled siRNA were transfected into HCC cell lines with Lipofectamine RNAiMAX (Invitrogen, Cat#13778-150) according to the manufacturer's instructions. After transfection for 48 h, cells were harvested for the validation of knockdown efficiency and subsequent functional experiments.

Clone formation assay and CCK-8 assay

For the clone formation assay, cells were cultured in 6-well plates (Corning, Cat#3516) at a density of 1000 cells per well and incubated for 2 weeks. The cells were fixed with 4% paraformaldehyde for 20 min at room temperature and finally stained with 0.1% crystal violet. The quantification of clone numbers was measured using ImageJ software (National Institutes of Health). CCK-8 kit (Beyotime, Cat#C0038) was utilized to evaluate the cell viability. Cells were seeded in 96-well plates (Corning, Cat#3599) at the density of 2000 cells per well and the Biotech-Epoch microplate reader was used to examine the optical density with a wavelength of 450 nm for five consecutive days.

Wound healing assay and cell migration assay

For the wound healing assay, cells were plated into 6-well plates (Corning, Cat#3516) until they reached confluence. The monolayer was then scratched by a tip, washed with PBS, and incubated with serum-free medium. Cells were photographed at 0 h and 24 h post-wounding. The

quantification of closure area was measured by ImageJ software (National Institutes of Health). For the cell migration assay, cells were seeded in the upper chambers with 100ul serum-free medium, and the lower chamber was filled with 600ul medium with 10% FBS. After incubation for 24 h, the cells on the bottom surface of the upper chamber were wash with PBS, fixed with 4% paraformaldehyde and stained with 0.1% crystal violet, and observed under the microscope.

QUANTIFICATION AND STATISTICAL ANALYSIS

The Student's t-test or Wilcoxon test was utilized to compare the statistical differences between groups. The Pearson Correlation Coefficient was applied to evaluate the relationship between various factors. All experiments were repeated independently an least three times ($n \geq 3$). Statistical analysis was performed and plotted using the R software (version 4.1.0) and GraphPad Prism software (version 8.0). Data were represented as mean +/- SEM. *P* value < 0.05 was defined as significant (*$p < 0.05$, **$p < 0.01$, ***$p < 0.001$, ****$p < 0.0001$).